Date:	22 Aug 2022
To:	"Narayan Bose" narayan.bghs@gmail.com
cc:	dsaha@isical.ac.in, sahad.geol@gmail.com, sahad.jess22@gmail.com, "Takeshi Imayama" imayama@ifst.ous.ac.jp, "Ryoichi Kawabata" s18sm03kr@ous.jp, "Saibal Gupta" saibl@gg.iitkgp.ac.in, "Keewook Yi" kyi@kbsi.re.kr
From:	"Dilip Saha" dsaha@isical.ac.in;sahad.geol@gmail.com;sahad.jess22@gmail.com
Subject:	JESS: Your manuscript entitled Intra-channel detachment in a collisional orogen: the Jhala Normal Fault in the Bhagirathi river section, Garhwal Higher Himalaya, India

Ref.:
Ms. No. JESS-D-22-00037R2
Intra-channel detachment in a collisional orogen: the Jhala Normal Fault in the Bhagirathi river section, Garhwal Higher Himalaya, India
Journal of Earth System Science

Dear Dr. Bose,

I am pleased to inform you that your manuscript has now been accepted for publication in Journal of Earth System Science. I hope the accompanying figures would be of good quality in the final version.

You will receive the proofs from the journal publishing office after your manuscript is scheduled for publication.

Thank you for submitting your manuscript to this journal.

Yours sincerely,

Dilip Saha, Ph.D.
Associate Editor
Journal of Earth System Science

****

Journal of Earth System Science

Intra-channel detachment in a collisional orogen: the Jhala Normal Fault in the Bhagirathi river section, Garhwal Higher Himalaya, India

--Manuscript Draft--

Manuscript Number:	JESS-D-22-00037R2
Full Title:	Intra-channel detachment in a collisional orogen: the Jhala Normal Fault in the Bhagirathi river section, Garhwal Higher Himalaya, India
Article Type:	Original Study
Keywords:	Poiseuille flow; U-Pb geochronology; South Tibetan Detachment; Miocene; Decompression melting
Corresponding Author:	Narayan Bose, Ph.D. Indian Institute of Technology Kharagpur INDIA
Corresponding Author Secondary Information:	
Corresponding Author's Institution:	Indian Institute of Technology Kharagpur
Corresponding Author's Secondary Institution:	
First Author:	Narayan Bose, Ph.D.
First Author Secondary Information:	
Order of Authors:	Narayan Bose, Ph.D.
	Takeshi Imayama
	Ryoichi Kawabata
	Saibal Gupta
	Keewook Yi
Order of Authors Secondary Information:	
Funding Information:	
Abstract:	In the Bhagirathi River Transect of the Garhwal Himalaya, India, the existence of the Jhala Normal Fault (JNF) and its movement sense are disputed. The JNF has been considered either as part of the South Tibetan Detachment System (STDS) or as a distinct, more southerly discontinuity within the Higher Himalayan Crystalline Sequence (HHCS). Field studies reveal that the JNF lies entirely within the HHCS, with both the JNF footwall and hanging-wall preserving thrust-related shear markers within amphibolite facies HHCS rocks. Rare extensional shear markers are, however, observed at the base of the JNF hanging-wall. New U-Pb zircon rim and monazite SHRIMP ages of 33.8 ± 0.8 Ma and 30.7 ± 0.5 Ma obtained in this study represent the timing of metamorphism in the JNF hanging-wall and footwall, respectively. Together, the field and geochronological evidence suggest that during Eocene-Oligocene channel flow in the HHCS, the slow-moving marginal part of the channel representing the JNF hanging-wall was trailing its more rapidly extruding footwall, resulting in apparent normal-sense movement across the JNF. The intrusion of 21.4 ± 2.3 Ma (monazite U-Pb age) tourmaline-bearing leucogranites within the JNF hanging-wall testifies to its ongoing uplift as part of the exhuming Miocene HHCS channel. The absence of any metamorphic break or distinct extensional shear zone at the JNF indicates that it originated as an intra-channel discontinuity rather than a major lithotectonic boundary.
Additional Information:	
Question	**Response**
Major Classification Term	1000.1.1: Tectonics

<p>Please indicate the Major Classification Term of your manuscript.This will help us finding the right handling editor for your submission. <p>Please copy and paste the entire text inclusive the numbering system into the text box below, e.g. if you selected <i>2000.1.2: Modelling</i> and <i>2000.1.3: Monsoons</i> in the previous step "Select Classifications", and the paper is primarily about modelling then please add <i>2000.1.2: Modelling</i> in the text box below.	1000.1.3: Geodynamics

Intra-channel detachment in a collisional orogen: the Jhala Normal Fault in the Bhagirathi river section, Garhwal Higher Himalaya, India

Narayan Bose[a,*], Takeshi Imayama[b], Ryoichi Kawabata[b], Saibal Gupta[a], Keewook Yi[c]

[a] Department of Geology and Geophysics, Indian Institute of Technology Kharagpur, Kharagpur 721302, West Bengal, India; narayan.bose@gg.iitkgp.ac.in (N.B.); saibl@gg.iitkgp.ac.in (S.G.)

[b] Frontier Institute of Science and Technology, Okayama University of Science, 7000005 Okayama, Japan; imayama@ifst.ous.ac.jp (T.I.); s18sm03kr@ous.jp (R.K.)

[c] Geochronology Team, Korea Basic Science Institute, 28119 Ochang, Republic of Korea; kyi@kbsi.re.kr (K.Y.)

[*] Corresponding author: narayan.bghs@gmail.com (N.B.), ORCID: 0000-0001-5395-0788

Abstract

In the Bhagirathi River Transect of the Garhwal Himalaya, India, the existence of the Jhala Normal Fault (JNF) and its movement sense are disputed. The JNF has been considered either as part of the South Tibetan Detachment System (STDS) or as a distinct, more southerly discontinuity within the Higher Himalayan Crystalline Sequence (HHCS). Field studies reveal that the JNF lies entirely within the HHCS, with both the JNF footwall and hanging-wall preserving thrust-related shear markers within amphibolite facies HHCS rocks. Rare extensional shear markers are, however, observed at the base of the JNF hanging-wall. New U-Pb zircon rim and monazite SHRIMP ages of 33.8 ± 0.8 Ma and 30.7 ± 0.5 Ma obtained in this study represent the timing of metamorphism in the JNF hanging-wall and footwall, respectively. Together, the field and geochronological evidence suggest that during Eocene-Oligocene channel flow in the HHCS, the slow-moving marginal part of the channel representing the JNF hanging-wall was trailing its more rapidly extruding footwall, resulting in apparent normal-sense movement across the JNF. The intrusion of 21.4 ± 2.3 Ma (monazite U-Pb age) tourmaline-bearing leucogranites within the JNF hanging-wall testifies to its ongoing uplift as part of the exhuming Miocene HHCS channel. The absence of any metamorphic break or distinct extensional shear zone at the JNF indicates that it originated as an intra-channel discontinuity rather than a major lithotectonic boundary.

Keywords: Poiseuille flow, U-Pb geochronology, South Tibetan Detachment, Miocene, Decompression melting

1. Introduction

The Himalayas, commonly accepted to have formed following the Cenozoic 54-50 Ma India-Eurasia collision (Najman *et al.*, 2017; Bhattacharya *et al.*, 2021), are characterised by orogen-wide litho-structural units separated by regional thrusts (Figure 1a). Sequentially to the south of the Indus Tsangpo Suture Zone (ITSZ), the major litho-structural units in the Himalayas are the Tethyan Sedimentary Sequence (TSS), the Higher Himalayan Crystalline Sequence (HHCS), the Lesser Himalayan Sequence (LHS) and the Siwalik Himalaya (SH). While the HHCS and the LHS are separated by the Main Central Thrust (MCT), the LHS is separated from the SH by the Main Boundary Thrust (MBT). The Main Frontal Thrust (MFT) defines the boundary between the SH and the Indo-Gangetic Plain and represents the southern limit of the Himalayan range. In contrast to the other discontinuities, the TSS and the HHCS are separated by an orogen-scale extensional shear zone called the South Tibetan Detachment System (STDS). The reason for the existence of an extensional discontinuity in a zone primarily characterised by crustal shortening has been a subject of considerable debate (e.g. Burchfiel *et al.* 1992; Hodges *et al.* 1992; see review by Kellett *et al.*, 2018). Some workers considered the STDS to have originated as an Eocene thrust (top-to-south) that was reactivated as a normal (top-to-north) fault during the Miocene (e.g. Ratsbatcher *et al.*, 1994; Aikman *et al.*, 2008; Kellett and Godin, 2009). An alternative 'channel flow' model proposed that the STDS originated during the extrusion of deep-seated metamorphic rocks along a low viscosity channel between the MCT and the STDS (e.g. Beaumont *et al.*, 2004, Jamieson *et al.*, 2004). Godin *et al.* (2006) considered the STDS to represent the boundary between the rheologically stronger upper crust and weaker middle crust. Irrespective of which model best explains the observations, these studies served to highlight the importance of the STDS in

Himalayan geodynamics and emphasised the necessity for its identification and characterisation in different sectors of the orogen.

Multiple criteria have been employed to identify and define the STDS, such as a *1.* sharp change in the metamorphic gradient from amphibolite facies to greenschist facies (Corrie *et al.* 2012; Long *et al.* 2017); *2.* persistent protolith boundary (Kellett & Grujic 2012; Greenwood *et al.* 2016); and *3.* presence of a top-to-north-down extensional shear zone (Searle 2010). However, as a shear zone may cut across protolith- and litho-tectonic boundaries, Kellett *et al.* (2018) suggested that the width of the STDS zone should be defined based on a structural feature, such as the appearance of penetrative top-to-north shear sense indicators along the transect; indeed, some workers have suggested that the width of a shear zone may be governed by a number of parameters (Cawood and Platt, 2021; Maity and Banerjee; 2022). Based on these assumptions, the STDS has been identified and subsequently dated (Finch *et al.*, 2014; Weinberg, 2016; Supplementary Table 1) in various sectors of the Himalayas, but its precise location in some transects remains disputed. Among these is the Bhagirathi Valley sector (Figure 1b), where a lithologic boundary associated with a prominent geomorphic feature in the northern part of the HHCS, referred to as the Jhala Normal Fault (JNF), was identified as the STDS (Agarwal and Kumar, 1973). A host of workers have identified the JNF either as a normal fault (e.g. Metcalfe, 1990, 1993; Searle *et al.*, 1993, 1999; Scaillet *et al.*, 1995) or a reverse fault (e.g. Valdiya, 1988; Sorkhabi *et al.*, 1999; Pêcher, 1991; Yin 2006), while some even question the very existence of a tectonic break at the location of the postulated JNF (e.g. Jain *et al.*, 2002, Catlos *et al.*, 2007). The status of the JNF, therefore, remains disputed. This study attempts to understand the nature of the JNF through a combined study of new field observations and SHRIMP geochronological data across the JNF. In particular, we discuss the evidence for the existence of normal sense-movement at the location of the JNF and re-evaluate the proposed correlation between the JNF and the STDS.

2. Geological background

In the Bhagirathi Valley sector, Agarwal and Kumar (1973) were the first to postulate a discontinuity at the JNF location, where almandine-amphibolite facies HHCS rocks are separated from greenschist facies meta-sediments of Martoli Formation (= Harsil Formation in Figure 1b) in the north. They also reported the presence of acid intrusives in the Martoli Formation only, i.e., not in the HHCS rocks present south of the JNF. The exact location of the JNF was demarcated by the sudden broadening of the river channel and landslides near the village Sukki (Figure 2). However, Manickavasagam *et al.* (1999) reported the presence of staurolite-kyanite grade HHCS rocks north of the JNF and plotted the STDS, locally known as Martoli Fault (MF, Figure 1b), at a more northerly location than the JNF. Subsequently, Metcalfe (1990) placed the JNF discontinuity at the river bend ~500 m north of the Jhala Bridge, where Agarwal and Kumar (1973) had initially located the JNF. He reported a prominent metamorphic break at the JNF as indicated by the change in lithology from kyanite-sillimanite bearing upper-amphibolite Vaikrita Group gneiss to upper greenschist/ lower amphibolite facies fine-grained psammite / meta-greywacke of Martoli Formation. Elongated lens-shaped assemblages containing hornblende and garnet inside the meta-greywacke were considered to be derived from marly pods. Extensive N-S extension was also postulated by Metcalfe (1990) primarily based on the field observation of shear folds. Although south-verging, he argued in favour of a normal (or extensional) shear component to be associated with these folds. Based on the muscovite closure temperature, Metcalfe (1993) predicted that the JNF was active till ~20 Ma. Supporting these observations, Searle (1993, 1999) proposed an extension-driven gravitational collapse model for the origin of the JNF, which was thought to be the southernmost member (splay) of an extensional shear zone system, i.e., the STDS.

In contrast, Prince (2000) discarded the presence of both a metamorphic break and an extensional shear zone at the JNF. However, a lithological boundary was marked by the augen gneiss in between the HHCS and the Harsil Formation (Figure 1), which is present north of the postulated JNF. According to Prince (2000), although the kyanite-garnet-staurolite-sillimanite bearing psammites-pelites of the Harsil Formation had a sedimentary origin, they could not be considered as a part of the unmetamorphosed TSS. Hence, according to him, the JNF does not represent the tectonic boundary between the HHCS and TSS (i.e., the STDS); rather, it is a gradational/ imbricated litho-boundary present inside the HHCS. These interpretations of Prince (2000) were supported by the work of Williams (2000), who presumed the JNF just to be a zone of strain localisation associated with the regional scale extensional shear zone (the STDS) present above. However, the exact location of the STDS in this transect remained uncertain due to restricted accessibility beyond Harsil. Discarding the presence of an extensional shear zone and a tectonic boundary at the JNF, Jain *et al.* (2002) placed the STDS (local name Martoli Fault; Figure 1b) at the contact between the Gangotri granite and the TSS. Mukherjee (2013) regarded the JNF as the lower boundary of the STDS shear zone, which extends into the upper parts of HHCS. Chambers (2008) reported an exceptional scenario at the JNF due to the lack of an adequately defined ductile extensional shear zone, which makes it difficult to correlate the JNF with the STDS. This confusion persists even in the most recent literature, with workers continuing to debate if the JNF is actually a part of the STDS (e.g. Sen *et al.*, 2021) or not (e.g. Kawabata *et al.*, 2021).

3. Methodology

3.1. Field and Microstructural observations

A traverse was taken across the JNF from locations L1 to L5 (Figure 2a), which covers the above-discussed postulated JNF locations and contains an ample amount of the footwall and hanging-wall parts. Hence, the field observations have been subdivided into three major groups, viz. the postulated 'footwall', 'fault zone', and 'hanging-wall', based on the previous works (e.g., Metcalfe, 1990) on the JNF. In some cases, the photographed features were present at an elevation/ position where we could not reach to put a scale. Scale bars have been put on such figures. Although the samples were collected mainly for geochronological analyses, pterographic studies have also been done to check the mineral assemblages and metamorphic grades.

3.2. Monazite and zircon geochronology

Monazite and zircon grains from kyanite-bearing migmatite and augen gneiss in the footwall of the JNF and leucogranite and kyanite-garnet schist in the hanging-wall of the JNF were separated using the standard heavy liquid technique (using sodium polytungstate; maximum specific weight 3.1) and were then handpicked under a binocular microscope at the Okayama University of Science, Japan. Monazite and zircon grains were mounted in epoxy with 44069 USGS monazite standard (ca. 425 Ma, Aleinikoff *et al.* 2006) and the FC1 zircon standard (ca. 1099 Ma, Paces and Miller 1993). Cathodoluminescence (CL) and back-scattered electron (BSE) images were obtained using the scanning electron microscopes JEOL 6610LV at the Korea Basic Science Institute (KBSI), Ochang, South Korea.

The monazite and zircon U–Pb ages were analysed using the SHRIMP IIe ion microprobe at the KBSI. The analytical procedures for SHRIMP dating were similar to those in Williams (1998) and Imayama *et al.* (2019). A 15–20 μm spot size was used for all analyses using a 1.5–2 nanoampere (nA) negative ion oxygen beam (O_2^-). The zircon standard SL13 was also used for the calibration of U concentrations. Data reduction, age calculations, and common Pb corrections were conducted using Isoplot 3.7 (Ludwig 2012). Common Pb for monazite was corrected using the ^{204}Pb. Common Pb for zircons yielding pre-Cenozoic age (core) and Cenozoic age (rim) was corrected using ^{204}Pb and ^{208}Pb, respectively.

4. Field observations and sampling

Footwall: At L1 (30°58'38" N, 78°41'47" E), kyanite-bearing migmatites (Figure 2b; sample: 1105-4A) of upper amphibolite facies conditions (Kawabata *et al.*, 2021), are intruded by a tourmaline-leucogranite (Figure 2c). Stromatic migmatites (Singh *et al.*, 2022) with deformed melt layers (Figure 2d; L2: 30°59'15" N, 78°41'59" E), migmatitic gneisses with folded bands (Figure 2e; L2: 30°59'40" N, 78°41'50" E), and augen gneisses (sample: 1105-7; Figure 2f; L3: 31°0'43" N, 78°42'27" E) are present in the upper part of the JNF footwall.

Fault zone: The zone lying between the augen gneisses at L3 and the meta-sedimentary Harsil Formation at L4 is the zone identified as the Jhala Normal Fault (JNF), although no fault plane *sensu stricto* is observed in the field. This zone is located near the Jhala Bridge, where abrupt widening of the river profile (see 'Discussions' for details) takes place. From the foliation (S0/S1) orientation (dipping 44° towards north) at this location, the JNF is considered to be a WNW-ESE trending discontinuity with a moderate northerly dip (e.g., Metcalfe, 1993). Hence, with respect to the JNF, the highly-sheared augen gneiss at L3 represents the top of the foot-wall block. Similarly, the base of the hanging-wall block is represented by the meta-sedimentary Harsil Formation rocks that lie north of the Jhala Bridge at L4. The proportion of felsic melts and shear intensity in the host rock is much more in the footwall rocks and abruptly decreases in the schists (Figures 3, 4) of the Harsil Formation (Metcalfe, 1990; Prince, 1999), i.e., north of the Jhala Bridge (Figure 2a) at L4 (31°1'1" N, 78°42'49" E).

Hanging-wall: In the JNF hanging-wall, a traverse has been taken from locations L4 (31°1'1" N, 78°42'49" E) to L5 (31°2'5" N, 78°44'48" E), as marked in Figure 2a. The major rock types in the Harsil Formation are biotite-bearing schists with abundant quartz veins that preserve evidence of deformation. Kyanite-garnet schists (sample: 1105-8C) and garnet-biotite±staurolite schists are also present. Biotite-rich mafic and quartzo-feldspathic segregations are still observed near the JNF (Figure 3a) but gradually diminish in proportion towards the north. Relicts of the S1 foliation are preserved as isoclinal folds (Figure 3b) or isolated fold hinges (Figure 3c), while the S2 foliation is pervasive throughout. Signatures of both layer parallel extension and layer perpendicular shortening are pervasive in this stretch (e.g., Figure 3d). Here, the sense of shear is mostly evident from structures in quartz veins. Boudins (Figure 4a), asymmetric folds (Figure 4b, c) and antithetic shears (Figure 4d) indicate a prominent top-to-south-up shear sense related to thrusting all along this transect. However, although much less abundant, top-to-north-down shear sense markers are also sporadically preserved in the sheared quartz veins (Figure 5a-d). Tourmaline-bearing leucogranites (Figure 6a; sample 1106-1D) intruded the Harsil Formation cutting across the host units at a low angle with the S2 foliation. This intrusion appeared to follow the fractures present in the host rock (Figure 6b-d), signifying the brittle nature of the latter during the intrusion.

5. Petrography and microstructure

The kyanite-bearing migmatites (Figure 7a, b) in the footwall (sample 1105-4A) indicate upper amphibolite facies condition. High-temperature (~700°C) microstructures such as chess-board extinction (Figure 7b) are present (Kruhl, 1996). In the hanging-wall (kyanite-garnet schist, sample 1105-8C), idiomorphic feldspar grains (Figure 7c) indicate static recrystallisation (Passchier and Trouw, 2005). The garnet-kyanite-biotite±staurolite assemblage, straight grain-boundaries of the idiomorphic grains and the strain-free texture are all consistent with equilibration under lower amphibolite facies conditions (Vernon, 2018). Some of the biotites appear to be mimetically recrystallised following older crenulations (Figure 7c), also suggesting a similar grade of metamorphism. This interpretation of lower-upper amphibolite facies condition is in agreement with the previously reported (Kawabata *et al.*, 2021) peak P-T conditions across the JNF, i.e., 7–9 kbar, 690–740°C in the footwall and 6.5 kbar, 620°C in the hanging-wall. The presence of aluminous minerals such as kyanite and staurolite indicates that the main rock type in the Harsil formation includes metapelites (for example, kyanite-garnet schist in Figure 7d).

6. Geochronology results

Results of monazite (Figure 8) and zircon (Figure 9) U–Pb analysis are listed in Supplementary Tables 2 and 3, respectively. The $^{206}Pb^{*}/^{238}U$ ages from each analytical spot are quoted at a 1σ confidence level, as shown in Supplementary Tables 2 and 3. A weighted mean $^{206}Pb^{*}/^{238}U$ ages in the text are quoted at a 2σ confidence level.

Monazite grains from kyanite-bearing migmatite (1105-4A) in the footwall of the JNF are rounded with irregular edges, with sizes of 80–120 μm. Clear zoning is not observed in the BSE image (Figure 8a, b). Metamorphic monazites yield the $^{206}Pb^{*}/^{238}U$ age range from 29.0 ± 1.0 to 32.9 ± 4 Ma (Figure 8c). Although some data have a large error due to a wide range of $^{207}Pb^{*}/^{235}U$ and $^{206}Pb^{*}/^{238}U$ ratios, the age is concentrated at ca. 30–31 Ma. A weighted mean $^{206}Pb^{*}/^{238}U$ age of 30.7 ± 0.5 Ma (MSDW = 0.48, 2σ) indicate the timing of metamorphism.

Zircon grains from augen gneiss (1105-7) in the footwall of the JNF are subhedral to euhedral with a large grain size up to 200 μm in diameter. The CL images of zircon grains show well-developed prismatic facies and internal oscillatory zoning (Figure 9a, b). The outer parts in zircons often have dark-CL domains with weakly oscillatory zoning formed by recrystallisation of pre-existing zircon. The zircon grains have a high Th/U ratio of 0.20–0.70. Most zircons yield the $^{207}Pb^{*}/^{206}Pb^{*}$ ages and $^{206}Pb^{*}/^{238}U$ ages of 572–454 Ma and 492–475 Ma, respectively (Figure 9f). A weighted mean of the $^{206}Pb^{*}/^{238}U$ ages is 485.8 ± 0.8 Ma (MSDW = 0.51, 2σ), representing a Cambrian-Ordovician age of the augen gneiss protolith. One spot yields the $^{206}Pb^{*}/^{238}U$ age of 516 Ma, which is interpreted as an inherited grain.

Monazite grains from tourmaline-bearing leucogranite (1106-1D) intruding the hanging-wall of the JNF are euhedral to subhedral, with sizes varying from 80–200 μm. Most monazite grains from the leucogranite are unzoned, and a few of them show weak concentric or patchy zoning (Figure 8d, e). Inherited grains were not identified. Magmatic monazites yield the $^{206}Pb^{*}/^{238}U$ age range from 26.2 ± 0.3 to 22.7 ± 0.3 Ma (Figure 8f). The data are slightly discordant, but lower intercepts of the discordia line yield a $^{206}Pb^{*}/^{238}U$ age of 21.4 ± 2.3 Ma (MSDW = 6.9, 2σ), interpreted to represent the time of emplacement of the leucogranite.

Most zircon grains from the kyanite-garnet schist (1105-8C) from the JNF hanging-wall are characterised by inherited detrital cores with bright-CL, surrounded by overgrown rims with dark-CL (Figure 9c-e). The inherited cores have high Th/U ratios of 0.03–0.56. Their $^{207}Pb^{*}/^{206}Pb^{*}$ ages of 1427-946 Ma are significantly older than the $^{206}Pb^{*}/^{238}U$ ages of 976–401 Ma (Figure 9g), indicating that the detrital grains were mainly derived from a Proterozoic terrane, whereas they were affected by Pb loss during later metamorphism. The overgrowing rims yield Himalayan ages (Figure 9h) with low Th/U ratios of 0.004-0.007. They yield $^{206}Pb^{*}/^{238}U$ ages from 35.4 Ma to

33.2 Ma, except for one domain that yields a $^{206}Pb^*/^{238}U$ age of 26.5 ± 0.4 Ma; the weighted mean of the $^{206}Pb^*/^{238}U$ ages is 33.8 ± 0.8 Ma (MSDW = 2.4, 2σ). Such a low Th/U ratio (less than 0.1) in zircon rims, compared to those of inherited zircon cores, is generally attributed to the growth of these rims during metamorphism (e.g., Rubatto, 2002; Imayama *et al.*, 2012), indicating that the metamorphism occurred at ca. 34 Ma.

7. Discussion

As mentioned earlier (Sections 1, 2), there is considerable disagreement about the existence of normal faulting or normal sense movement along the JNF. No prominent brittle- or ductile-extensional shear zone or break in metamorphic grade is observed at the location of the JNF. Rather, thrusting related top-to-S/SW-up shear-sense markers dominate the region across the JNF. This is in agreement with the observations of Prince (1999), Williams (2000), Catlos *et al.* (2007) and Chambers (2008), who also did not observe any significant normal sense markers at the postulated location of the JNF. Across the JNF, the P–T conditions decrease gradually from upper amphibolite facies to lower amphibolite facies metamorphism, and there is no sharp change in the metamorphic gradient (see also Kawabata *et al.*, 2021). Moreover, the kyanite-bearing schists in the JNF hanging wall show lithological affinity with the lower HHCS (Kawabata *et al.*, 2021). In addition, the garnet zoning pattern in both hanging-wall and footwall preserves patterns characteristic of diffusional zoning with retrograde rims (Kawabata *et al.*, 2021), which is a typical garnet zoning pattern in the HHCS (e.g., Imayama *et al.*, 2010). Additionally, the greywacke/ shale/ calcareous sedimentary rocks, characteristic of the TSS (Valdiya, 1988), are absent from the Harsil Formation. Hence, due to the absence of any metamorphic break at the JNF, this discontinuity cannot be considered as the boundary between the HHCS and the TSS (i.e., the

STDS). However, a few ductile extensional features are indeed observed (e.g. Figure 5) at the base of the Harsil Formation, i.e., in the JNF hanging-wall. Although these can be explained by the rotation of the stress field during thrusting (Simpson and De Paor, 1993; review by Dutta and Mukherjee, 2019), these do suggest that the inference of normal-sense movement along the JNF cannot be completely discarded, since such extensional features are entirely absent in the footwall. Thus, it appears that the base of the Harsil Formation did experience an extensional component (see also Williams, 2000), which possibly overprinted earlier thrusting. As argued below, this may be explicable in terms of the velocity gradient at the margins of an extruding channel.

7.1. Geodynamic evolution of the JNF: Is there any 'normal faulting' at the JNF?

As the JNF hanging-wall is a part of the HHCS, ductile deformation in this unit is most likely the result of channel flow extrusion of the HHCS (e.g. Beaumont *et al.*, 2001). Channel flow concepts have been employed previously to explain the normal movement at the STDS (e.g., Finch, 2014). A dominantly Poiseuille flow (or pipe flow) mechanism, along with a Couette flow component, has been hypothesised to be the governing flow pattern in the channel (e.g. Godin *et al.*, 2006; Grujic, 2006). In the general case of Poiseuille flow, material velocity is maximum at the centre and gradually diminishes towards the margins of the channel. In their model, Grujic *et al.* (2002) predicted the presence of a discontinuity ("STD" in their model) near the upper margin of the channel. The earlier authors also suggested that the region above this discontinuity would experience much less displacement compared to the central part of the channel, which has higher material velocity. In the present study, although the JNF has been demonstrated to be located within the HHCS, the presence of a discontinuity within the channel (Figure 10a) may be visualised from the following arguments: 1. Being the topmost part of the channel, the JNF hanging-wall dissipated heat to the overlying TSS and cooled faster than the warmer central part. This resulted in a rheological contrast across the JNF; 2. Flow velocities in the marginal part of the channel were reduced due to the drag of the overlying block (i.e., STDS hanging-wall), 3. There may have been a pre-existing weakness at the JNF location under the influence of the nearby STDS and related damage zones. With this rationale, the evolution of structures across the JNF can be envisaged in three phases:

Phase 1 (pre-JNF): Ductile deformation in the JNF hanging-wall part was active from the Early Eocene India-Eurasia collision to the Late Eocene (Catlos *et al.*, 2020). The present study shows that the metamorphism just above (i.e., immediately north of) the JNF occurred at ~ 34 Ma. Considering the metamorphic zircon ages of 33.9 ± 1.2 Ma from kyanite-bearing migmatite in the footwall (Kawabata *et al.*, 2021), the timings of high-grade metamorphism in the hanging-wall and footwall also closely follow each other. On the other hand, a longer duration of high-temperature metamorphism during the Late Eocene-Early Miocene in the footwall, in contrast to the hanging wall, was constrained from compiled data of monazite and zircon ages (Figure 1, Kawabata *et al.*, 2021 and references therein) which is consistent with the monazite age of ca. 30.7 Ma in the footwall from this study. These data imply that the hanging-wall cooled earlier than the footwall. Following the origin of the discontinuity at the JNF (either by heat loss/ drag/ both as discussed above), the ductile deformation (thrusting) and channel-flow-related movement in the JNF hanging-wall ceased at ~ 34 Ma. However, channel flow continued in the southern parts of the JNF as evidenced by their younger (than 34 Ma) ages (compiled in Figure 1).

Phase 2 (syn-JNF): Unlike in the hanging-wall, the top of the footwall continued to experience metamorphic conditions in the amphibolite facies up to ~30.7 Ma. Higher temperatures were sustained for a longer duration in the footwall, indicating that the warmer footwall remained an active part of the extruding channel at this time, although the adjacent cooler hanging-wall does not preserve ages younger than 33 Ma. Continuing extrusion of material in the footwall relative to the hanging-wall would result in an apparent extensional displacement across the JNF. As a result, the amount of decompression melting and shear intensity is higher in the footwall than in the hanging-wall (e.g., Harris and Massey, 1994). It is likely that the drag exerted on the JNF hanging-wall by the overlying TSS acted as a resistance against the exhumation of the hanging-wall material. In such a scenario, where the footwall block moved up *with respect to* the hanging-wall, it results in an apparent 'normal fault' at the location of the JNF, in spite of the prevalence of thrust-sense markers across this discontinuity. In this respect, considering that the concerned deformation took place in the ductile regime, the term 'normal shearing' is more appropriate than 'normal faulting' at the JNF. There may be several such pulses of differential movement within the channel (e.g., Hollister and Grujic, 2006), which may also be accompanied by subsequent gravitational collapse (Figure 10a).

Phase 3 (post-JNF): The next major phase of deformation at the JNF took place during the Early Miocene with the rapid exhumation of the HHCS, coeval with the normal faulting at the STDS. During this phase, the whole HHCS wedge (including both the JNF hanging-wall and foot-wall) was uplifted with respect to the Tethyan Sedimentary Sequence (Figure 10b). The ~21.4 Ma emplacement of the tourmaline-bearing leucogranites in the uplifted block (i.e., the STDS footwall) is coeval with the extension at the STDS (Figure 1 for ages).

7.1.1. Abrupt change in river profile: probable significance

The sudden change in the river profile at the Jhala bridge is intriguing and indeed is responsible for much of the controversy regarding the nature and existence of the JNF. Different river incision rates due to variable rates of uplift are a common feature of a tectonically active region (Kirby and Whipple, 2012). In the current study area, the sudden change in the width of the river (Bhagirathi) channel at the JNF seems to testify to the presence of a normal fault, where the southern block (i.e., footwall) is relatively more uplifted. Although beyond the scope of the current study, geomorphological parameters have been proven to be useful in identifying the presence of faults intersected by river channels (e.g., Rawat *et al.*, 2022). However, knick points are present (Figure 2g) on the Bhagirathi river channel near the Jhala bridge, i.e., the postulated location of the JNF. The absence of brittle shear signatures (as discussed above) may indicate the inactive nature of the present-day JNF. Hence, the sudden change in the valley profile (Figure 2) and the knick points near the JNF cannot be attributed to the recent activity of the JNF. But, as discussed above, the rate of exhumation across the JNF was different in the Early Miocene, resulting in an apparent normal-sense displacement at the location of the JNF. This variable displacement is likely to bring rocks of sharply contrasting erosivity into juxtaposition across the discontinuity. Thus, the presence of rocks with different erosivity (Montogomery and Gran, 2001) across the JNF might have triggered the sudden change in the valley profile following the exhumation of the rocks at this location.

7.2. Regional significance of the JNF: Is the JNF a part of the STDS or not?

The tectonothermal event associated with the JNF (~ 33.8 Ma) operated much earlier than the extension at the nearby STDS (~20 Ma; e.g., Montemagni *et al.*, 2018). Section 7.1 discusses how the JNF originated as an intra-HHCS discontinuity during channel-flow extrusion of the footwall. Similar discontinuities have been reported from other parts of the Himalayas as well. For example, in the HHCS of the W. Bhutan, Carosi *et al.* (2006) report a pure-shear dominated normal shear zone, which operated during the 20-17 Ma channel flow extrusion. Again, from the Himachal HHCS (NW Himalaya), Stübner *et al.* (2014) report deep crustal partial melts that were generated during the 37–36 Ma peak metamorphism (~8–8.5 kbar, ~600–700 °C).

However, observations from many parts of the Himalayas also suggest that a discontinuity was generated at the top of the HHCS during the STDS activation. For example, the extension along the Higher Himalayan shear zones at Yadong and Nyalam was initiated respectively at ~28 Ma and ~22 Ma in Pulan, which are coeval with the activity of the STDS in those areas (Xu *et al.*, 2013). The STDS is fundamentally defined as an Eocene thrust that was reactivated as a normal fault during the Miocene. The JNF also has a similar evolutionary history (Eocene thrusting, followed by Miocene normal faulting). Additionally, two-mica leucogranite (early phase of decompression melting) is present at the top of the footwall of both the STDS (as Bhaironghati gneiss; Figure 1) and the JNF (Figure 2). Hence, the mechanism of deformation of the STDS and the JNF show some similarities in spite of the age gap. Summarily, extension along the JNF and MF were initiated as two separate events, and hence the JNF did not originate as a part of the STDS. It is suggested that differential movement within the channel was responsible for the apparent extensional displacement at the JNF. On the other hand, the MF actually separates high-grade HHCS rocks from the TSS and experiences extension under the influence of gravity collapse. Thus, these observations suggest another mechanism of inception and development of detachments within a ductile extruding channel during major orogenic events.

8. Conclusions

The Jhala Normal Fault (JNF) in the Bhagirathi River section is postulated to pass through a location where highly sheared augen gneisses of the Higher Himalayan Crystalline Sequence

(HHCS) changes to kyanite-garnet schist and biotite psammitic schist of the Harsil formation near the Jhala Bridge. Integration of field observations, microstructures and age data demarcate three major events related to the JNF evolution. Thrusting-related structures are observed across the postulated JNF location, although some extensional markers suggest limited normal-sense movement at the base of the JNF hanging-wall. Following the peak metamorphism at ~34 Ma, the JNF hanging-wall was gradually detached from the more active central part of the HHCS channel, whereas the high-grade metamorphism continued in the footwall till ~30.7 Ma. This testifies to an apparent extensional displacement across the JNF during ~30.7 Ma when the footwall material moved upward faster than the hanging-wall. Finally, at ~21.4 Ma, the normal movement of the STDS triggered the intrusion of tourmaline-bearing leucogranites into the JNF hanging-wall. This study suggests that the JNF was most likely an intra-channel detachment rather than the channel margin (i.e., the STDS), as suggested in some previous studies.

Acknowledgements: The research was supported in part by Grant No. 18K03788 to T.I. from the Japan Society for the Promotion of Science. This research was also supported by the Korea Basic Science Institute under the R&D program (Project No. D38700) to K.Y. from the Ministry of Science and ICT, Republic of Korea. N.B. thanks for the support extended by the Department of Geology and Geophysics, IIT Kharagpur, India. The authors thank Shinae Lee for helping during the SHRIMP analyses. The manuscript has greatly improved by the comments received from Sayandeep Banerjee (BHU, Varanasi), another anonymous reviewer and the Handling Editor Dilip Saha.

Author statement: Conceptualisation, N.B. and T.I.; methodology, N.B. and T.I.; software, T.I. and R.K.; validation, T.I. and R.K.; formal analysis, T.I., N.B., S.G., R.K. and K.Y.; investigation, T.I. and N.B.; resources, T.I. and K.Y.; data curation, N.B. and T.I.; writing—original draft preparation, N.B.; writing—review and editing, N.B., S.G. and T.I.; visualisation, N.B. and T.I.; supervision, N.B. and T.I.; project administration, T.I.; funding acquisition, T.I. and K.Y. All authors have read and agreed to the published version of the manuscript.

References

Agarwal N C and Kumar G 1973 Geology of the Upper Bhagirathi and Yamuna Valleys, Uttarkashi District, Kumaun Himalaya; *Himal. Geol.* **3** 2-23.

Aikman A B, Harrison T M and Lin D 2008 Evidence for early (>44 Ma) Himalayan crustal thickening, Tethyan Himalaya, southeastern Tibet; *Earth Planet. Sc. Lett.* **274** 14–23.

Aleinikoff J N, Schenck W S, Plank M O, Srogi L, Fanning C M, Kamo S L and Bosbyshell H 2006 Deciphering igneous and metamorphic events in high-grade rocks of the Wilmington Complex, Delaware: Morphology, cathodoluminescence and back-scattered electron zoning, and SHRIMP U-Pb geochronology of zircon and monazite; *Geol. Soc. Am. Bull.* **118** 39-64.

Beaumont C, Jamieson R A, Nguyen M H and Lee B 2001 Himalayan tectonics explained by extrusion of a low-viscosity crustal channel coupled to focused surface denudation; *Nature* **414(6865)** 738-742.

Beaumont C, Jamieson R A, Nguyen M H. and Medvedev S. 2004 Crustal channel flows: 1. Numerical models with applications to the tectonics of the Himalayan- Tibetan orogen; *J. Geophys. Res.-Sol. Ea.* **109** B06406.

Bhattacharya G, Robinson D M and Wielicki M M 2021 Detrital zircon provenance of the Indus Group, Ladakh, NW India: Implications for the timing of the India-Asia collision and other syn-orogenic processes; *Geol. Soc. Am. Bull.* **133(5-6)** 1007-1020.

Burchfiel B C and Royden L H 1985 North–south extension within the convergent Himalayan region; *Geology* **13** 679–682.

Burchfiel B C, Zhiliang C, Hodges K V, Yuping L, Royden L H, Changrong D and Jiene X 1992 The South Tibetan Detachment System, Himalayan Orogen: Extension Contemporaneous with and Parallel to Shortening in a Collisional Mountain Belt; *Geol. S. Am. S.* **269** 1-41.

Carosi R, Lombardo B, Molli G, Musumeci G and Pertusati P C 1998 The South Tibetan detachment system in the Rongbuk valley, Everest region. Deformation features and geological implications; *J. Asian Earth Sci.* **16(2-3)** 299-311.

Carosi R, Montomoli C, Iaccarino S, Massonne H J, Rubatto D, Langone A, Gemignani L and Visonà D 2016 Middle to late Eocene exhumation of the Greater Himalayan Sequence in the Central Himalayas: Progressive accretion from the Indian plate; *Geol. Soc. Am. Bull.* **128(11-12)** 1571-1592.

Carosi R, Montomoli C, Rubatto D and Visona D 2006 Normal-sense shear zones in the fore of the Higher Himalayan Crystallines (Bhutan Himalaya): Evidence for extrusion? *in* Law R D, Searle M P and Godin L (eds) Channel Flow, Ductile Extrusion and Exhumation in Continental Collision Zones; *Geol. Soc. London Sp. Pub.* **268** 425–444.

Catlos E J, Perez T, Lovera O, Dubey C S, Schmitt A K and Etzel T M 2020 High- resolution P-T- time paths across Himalayan faults exposed along the Bhagirathi Transect NW India: Implications for the construction of the Himalayan orogen and ongoing deformation; *Geochem. Geophy. Geosy.* **21** e2020GC009353.

Catlos E J, Dubey C S, Marston R A and Harrison T M 2007 Geochronologic constraints across the Main Central Thrust shear zone, Bhagirathi River (NW India): Implications for Himalayan tectonics; *Geol. S. Am. S.* **419** 135–151.

Cawood T K and Platt J P 2021 What controls the width of ductile shear zones; *Tectonophysics* **816** 229033.

Chambers J A 2008 Thermal evolution of the mid-crust from the Himalayan orogen; Ph.D. thesis, The Open University, UK, 304 p.

Corrie S L, Kohn M J, McQuarrie N and Long S P 2012 Flattening the Bhutan Himalaya; *Earth Planet. Sc. Lett.* **349** 67-74.

Dutta D and Mukherjee S 2019 Opposite shear senses: Geneses, global occurrences, numerical simulations and a case study from the Indian western Himalaya; *J. Struct. Geol.* **126** 357-392.

Finch M, Hasalová P, Weinberg R F and Fanning C M 2014 Switch from thrusting to normal shearing in the Zanskar shear zone, NW Himalaya: Implications for channel flow; *Geol. Soc. Am. Bull.* **126(7-8)** 892-924.

Godin L, Grujic D, Law R D and Searle M P 2006 Channel flow, ductile extrusion and exhumation in continental collision zones: an introduction. *in* Law R, Searle M P and Godin L (eds) Channel Flow, Ductile Extrusion and Exhumation in Continental Collision Zones; *Geol. Soc. London Sp. Pub.* **268** 1–23.

Godin L, Parrish R R, Brown R L and Hodges K V 2001 Crustal thickening leading to exhumation of the Himalayan metamorphic core of central Nepal: Insight from U- Pb geochronology and 40Ar/39Ar thermochronology; *Tectonics* **20(5)** 729-747.

Greenwood L V, Argles T W, Parrish R R, Harris N B and Warren C 2016 The geology and tectonics of central Bhutan; *J. Geol. Soc. London* **173** 352–369.

Grujic D 2006 Channel flow and continental collision tectonics: an overview. *in* Law R, Searle M P and Godin L (eds) Channel Flow, Ductile Extrusion and Exhumation in Continental Collision Zones. *Geol. Soc. London Sp. Pub.* **268** 25-37.

Grujic D, Hollister L S and Parrish R R 2002 Himalayan metamorphic sequence as an orogenic channel: insight from Bhutan; *Earth Planet. Sc. Lett.* 198 177–191.

Guillot S, Hodges K, Fort P L and Pêcher A 1994 New constraints on the age of the Manaslu leucogranite: Evidence for episodic tectonic denudation in the central Himalayas; *Geology* **22(6)** 559-562.

Guillot S, Mahéo G, de Sigoyer J, Hattori K H and Pecher A 2008 Tethyan and Indian subduction viewed from the Himalayan high-to ultrahigh-pressure metamorphic rocks; *Tectonophysics* **451(1-4)** 225-241.

Harris N and Massey J 1994 Decompression and anatexis of Himalayan metapelites; *Tectonics* **13(6)** 1537-1546.

Harris N B W, Caddick M, Kosler J, Goswami S, Vance D and Tindle A G 2004 The pressure–temperature–time path of migmatites from the Sikkim Himalaya; *J Metamorph. Geol.* **22(3)** 249-264.

Hodges K V, Parrish R R, Housh T B, Lux D R, Burchfiel B C, Royden L H and Chen Z 1992 Simultaneous Miocene Extension and Shortening in the Himalayan Orogen; *Science* **258** 1466–1470.

Hollister L S and Grujic D 2006. Pulsed channel flow in Bhutan; *in*: Law R D, Searle M and Godin L (eds) Channel Flow, Extrusion and Exhumation of Lower-mid Crust in Continental Collision Zones; *Geol. Soc. London Sp. Pub.* **268** 415–423.

Iaccarino S, Montomoli C, Carosi R, Montemagni C, Massonne H J, Langone A, Jain A K and Visonà D 2017 Pressure- temperature- deformation- time constraints on the South Tibetan detachment system in the Garhwal Himalaya (NW India); *Tectonics* **36(11)** 2281-2304.

Imayama T, Arita K, Fukuyama M, Yi K and Kawabata R 2019 1.74 Ga crustal melting after rifting at the northern Indian margin: investigation of mylonitic orthogneisses in the Kathmandu area, central Nepal; *Int. Geol. Rev.* **61(10)** 1207-1221.

Imayama T, Takeshita T, Yi K, Cho D L, Kitajima K, Tsutsumi Y, Kayama M, Nishido H, Okumura T, Yagi K, Itaya T and Sano Y 2012 Two-stage partial melting and contrasting cooling history within the Higher Himalayan Crystalline Sequence in the far-eastern Nepal Himalaya; *Lithos* **134** 1-22.

Inger S 1998 Timing of an extensional detachment during convergent orogeny: New Rb-Sr geochronological data from the Zanskar shear zone, northwestern Himalaya; *Geology* **26(3)** 223-226.

Jain A K, Singh S and Manickavasagam R M 2002 Himalayan Collisional Tectonics; *Gondwana Res. Group Mem.* **7** Field Science Publishers Hashimoto 119p.

Jamieson R A, Beaumont C, Medvedev S and Nguyen M H 2004 Crustal channel flows: 2. Numerical models with implications for metamorphism in the Himalayan- Tibetan orogen; *J. Geophys. Res.-Sol. Ea* **109** B06407.

Kawabata R, Imayama T, Bose N, Yi K and Kouketsu Y 2021 Tectonic discontinuity, partial melting and exhumation in the Garhwal Himalaya (Northwest India): Constrains from spatial and temporal pressure-temperature conditions along the Bhagirathi valley; *Lithos* **404** 106488.

Kellett D A and Godin L 2009 Pre-Miocene deformation of the Himalayan superstructure, Hidden valley, central Nepal; *J. Geol. Soc. London* **166(2)** 261-275.

Kellett D A, Cottle J M and Larson K P 2018 The South Tibetan Detachment System: History, advances, definition and future directions; *in* Treloar P J and Searle M P (eds) Himalayan Tectonics: A Modern Synthesis; *Geol. Soc. London Sp. Pub.* **483** 377-400.

Kellett D A and Grujic D 2012 New insight into the South Tibetan detachment system: not a single progressive deformation; *Tectonics* 31 TC2007.

Kirby E and Whipple K X 2012 Expression of active tectonics in erosional landscapes; *J. Struct. Geol.* **44** 54-75.

Kruhl J H 1996 Prism- and basal- plane parallel subgrain boundaries in quartz: A microstructural geothermobarometer. *J. Metamorph. Geol.* **14(5)** 581-589.

Lin C, Zhang J, Wang X, Putthapiban P, Zhang B and Huang T 2020 Oligocene initiation of the south Tibetan detachment system: Constraints from syn-tectonic leucogranites in the Kampa dome, northern Himalaya; *Lithos* **354** 105332.

Long S P, Gordon S M and Soignard E 2017 Distributed north-vergent shear and flattening through Greater and Tethyan Himalayan rocks: insights from metamorphic and strain data from the Dang Chu region, central Bhutan; *Lithosphere* **9** 774–795.

Ludwig K R 2012 Isoplot/Ex rev. 3.75 – A Geochronological Toolkit for Microsoft Excel. *Berkeley Geochronology Center Sp. Pub.* **5** 75pp.

Maity S and Banerjee S 2022 Structural Anatomy of the Intraterrane Shear Zones in the Archean Bundelkhand Craton, North-Central India and Its Possible Linkage to Supercontinent Assembly: Insights from Field-and AMS-Based Kinematic Analysis; *Lithosphere* **2021(6)** 1-19.

Manickavasagam R M, Jain A K, Singh S, Asokan A, Macfarlane A, Sorkhabi R and Quade J 1999 Metamorphic evolution of the northwest Himalaya, India: Pressure-temperature data, inverted metamorphism, and exhumation in the Kashmir, Himachal, and Garhwal Himalayas; *Geol. S. Am. S.* **328** 179-198.

Metcalfe R P 1990 A thermotectonic evolution for the main central thrust and higher Himalaya, western Garhwal, India; PhD thesis, University of Leicester 231 pp.

Metcalfe R P 1993 Pressure, temperature and time constraints on metamorphism across the Main Central thrust zone and High Himalayan slab in the Garhwal Himalaya. *in* Treloar P J and Searle M P (eds) Himalayan tectonics; *Geol. Soc. London Sp. Pub.* **74** 485–509.

Montemagni C, Carosi R, Fusi N, Iaccarino S, Montomoli C, Villa I M and Zanchetta S 2020 Three- dimensional vorticity and time- constrained evolution of the Main Central Thrust zone, Garhwal Himalaya (NW India); *Terra Nova* **32(3)** 215-224.

Montemagni C, Iaccarino S, Montomonli C, Carosi R, Jain A K and Villa I M 2018 Age constraints on the deformation style of the South Tibetan Detachment System in Garhwal Himalaya; *Ital. J. Geosci.* **137(2)** 175-187.

Montgomery D R and Gran K B 2001 Downstream variations in the width of bedrock channels; *Water Resour. Res.* **37** 1841–1846.

Montomoli C, Carosi R, Rubatto D, Visonà D and Iaccarino S 2017 Tectonic activity along the inner margin of the South Tibetan Detachment constrained by syntectonic leucogranite emplacement in Western Bhutan; *Ital. J. Geosci.* 136(1) 5-14.

Mukherjee S 2013 Higher Himalaya in the Bhagirathi section (NW Himalaya, India): its structures, backthrusts and extrusion mechanism by both channel flow and critical taper mechanisms; *Int. J. Earth Sci.* **102(7)** 1851-1870.

Najman Y, Jenks D, Godin L, Boudagher-Fadel M, Millar I, Garzanti E, Horstwood M and Bracciali L 2017 The Tethyan Himalayan detrital record shows that India–Asia terminal collision occurred by 54 Ma in the Western Himalaya; *Earth Planet. Sc. Lett.* **459** 301-310.

Nania L, Montomoli C, Iaccarino S, Leiss B and Carosi R 2022 Multi-stage evolution of the South Tibetan Detachment System in central Himalaya: Insights from carbonate-bearing rocks; *J Struct. Geol.* **158** 104574.

Paces J B and Miller Jr J D 1993 Precise U- Pb ages of Duluth complex and related mafic intrusions, northeastern Minnesota: Geochronological insights to physical, petrogenetic, paleomagnetic, and tectonomagmatic processes associated with the 1.1 Ga midcontinent rift system; *J. Geophys. Res.-Sol. Ea.* **98(B8)** 13997-14013.

Passchier C W and Trouw R A 2005 Microtectonics (second ed); Springer Berlin, 366 pp.

Pêcher A 1991 The contact between the Higher Himalaya Crystallines and the Tibetan Sedimentary Series: Miocene large- scale dextral shearing; *Tectonics* **10(3)** 587-598.

Prince C I 1999 The timing of prograde metamorphism in the Garhwal Himalaya, India; PhD Thesis, Open University, 308 pp.

Ratschbacher L, Frisch W, Liu G and Chen C 1994 Distributed deformation in southern and western Tibet during and after the India- Asia collision; *J. Geophys. Res.-Sol. Ea* **99(B10)** 19917-19945.

Rawat A, Banerjee S, Sundriyal Y and Rana V 2022 An integrated assessment of the geomorphic evolution of the Garhwal synform: Implications for the relative tectonic activity in the southern part of the Garhwal Himalaya; *J. Earth Syst. Sci.* **131(1)** 1-25.

Rubatto D 2002 Zircon trace element geochemistry: partitioning with garnet and the link between U–Pb ages and metamorphism; *Chem. Geol.* **184(1-2)** 123-138.

Scaillet B, Pêcher A, Rochette P and Champenois M 1995 The Gangotri granite (Garhwal Himalaya): laccolithic emplacement in an extending collisional belt; *J Geophys. Res.* **100(B1)** 585–607.

Schärer U, Xu R H and Allègre C J 1986 U (Th) Pb systematics and ages of Himalayan leucogranites, South Tibet. *Earth Planet. Sci Lett.* **77(1)** 35-48.

Searle M P, Metcalfe R P, Rex A J and Norry M J 1993 Field relations, petrogenesis and emplacement of the Bhagirathi leucogra-nite, Garhwal Himalaya. *in* Treloar P J and Searle M P (eds) Himalayan tectonics; *Geol. Soc. London Sp. Pub.* **74** 429–444.

Searle M P, Noble S R, Hurford A J and Rex D C 1999 Age of crustal melting, emplacement and exhumation history of the Shivling leucogranite, Garhwal Himalaya; *Geol. Mag.* **136** 513–525.

Searle M P, Simpson R L, Law R D, Parrish R R and Waters D J 2003 The structural geometry, metamorphic and magmatic evolution of the Everest massif, High Himalaya of Nepal–South Tibet; *J. Geol. Soc. London* **160(3)** 345-366.

Searle M P 2010 Low-angle normal faults in the compressional Himalayan orogen; Evidence from the Annapurna–Dhaulagiri Himalaya, Nepal; *Geosphere* **6** 296–315.

Sen A, Sen K, Chatterjee A, Choudhary S and Dey A 2021 Understanding pre-and syn-orogenic tectonic evolution in western Himalaya through age and petrogenesis of Palaeozoic and Cenozoic granites from upper structural levels of Bhagirathi Valley, NW India; *Geol. Mag.* **159** 97-123.

Sen A, Sen K, Srivastava H B, Singhal S and Phukon P 2018 Age and geochemistry of the Paleoproterozoic Bhatwari Gneiss of Garhwal Lesser Himalaya, NW India: implications for the pre-Himalayan magmatic history of the Lesser Himalayan basement rocks. *in* Sharma R, Villa I M and Kumar S (eds) Crustal Architecture and Evolution of the Himalaya-Karakoram-Tibet Orogen; *Geol. Soc. London Sp. Pub.* **481(1)** 319-339.

Sen K, Chaudhury R and Pfänder J 2015 40Ar–39Ar age constraint on deformation and brittle–ductile transition of the Main Central Thrust and the South Tibetan Detachment zone from Dhauliganga valley, Garhwal Himalaya, India; *J Geodyn.* **88** 1-13.

Simpson C and De Paor D G 1993 Strain and kinematic analysis in general shear zones; *J Struct. Geol.* **15(1)** 1-20.

Singh S 2019 Protracted zircon growth in migmatites and in situ melt of Higher Himalayan Crystallines: U–Pb ages from Bhagirathi Valley, NW Himalaya, India; *Geosci. Front.* **10(3)** 793-809.

Singh S, Rit B, Mohan S P and Kushwaha A 2022) Crustal Melting Evidence in Migmatites of Higher Himalayan Crystallines (HHC) along Bhagirathi, Dhauliganga Valleys, and Sikkim Himalaya, India; *J. Geol. Soc. India* **98(1)** 69-73.

Sorkhabi R B, Stump E, Foland K and Jain A K 1999 Tectonic and cooling history of the Garhwal Higher Himalaya (Bhagirathi Valley): constraints from thermochronological data. *in* Jain A K, Manickavasagam R M (eds) Geodynamics of the NW Himalaya; *Gondwana Res. Gr. Mem.* **6** 217–235.

Sorkhabi R B, Stump E, Foland K A and Jain A K 1996 Fission-track and 40Ar39Ar evidence for episodic denudation of the Gangotri granites in the Garhwal Higher Himalaya, India; *Tectonophysics* **260(1-3)** 187-199.

Stern C R, Kligfield R, Schelling D, Fruta K and Virdi N S 1989 The Bhagirathi leucogranite of the High Himalaya, age, petrogenesis and tectonic im- plication; *Geol. S. Am. S.* **232** 33- 45.

Stübner K, Grujic D, Parrish R R, Roberts N M, Kronz A, Wooden J and Ahmad T 2014 Monazite geochronology unravels the timing of crustal thickening in NW Himalaya; *Lithos* **210** 111-128.

Valdiya K S 1988 Tectonics and evolution of the central sector of the Himalaya; *Philos. Tr. R. Soc. S-A* **326(1589)** 151-175.

Vannay J C and Hodges K V 1996 Tectonometamorphic evolution of the Himalayan metamorphic core between the Annapurna and Dhaulagiri, central Nepal; *J. Metamorph. Geol.* **14(5)** 635-656.

Vernon R H 2018 A practical guide to rock microstructure (2nd ed) Cambridge University Press, Cambridge 431 pp.

Weinberg R F 2016 Himalayan leucogranites and migmatites: nature, timing and duration of anatexis; *J Metamorph. Geol.* **34(8)** 821-843.

Williams H M 2000 Magmatic and tectonic evolution of Southern Tibet and the Himalaya; PhD thesis, Open University, 339 pp.

Williams I S 1998 U-Th-Pb geochronology by ion microprobe. *in* McKibben M A, Shanks III W C and Ridley W I (eds) Applications of microanalytical techniques to understanding mineralising processes; *Rev. Econ. Geol.* **7** 1-35.

White R W, Powell R, Holland T J B and Worley B A 2000 The effect of TiO2 and Fe2O3 on metapelitic assemblages at greenschist and amphibolite facies conditions: mineral equilibria calculations in the system K2O-FeO-MgO-Al2O3-SiO2-H2O-TiO2-Fe2O3; J. Metamorph. Geol. **18(5)** 497-511.

Xu Z, Wang Q, Pecher A, Liang F, Qi X, Cai Z, Li H, Zeng L and Cao H 2013 Orogen- parallel ductile extension and extrusion of the Greater Himalaya in the late Oligocene and Miocene; *Tectonics* **32(2)** 191-215.

Yin A 2006 Cenozoic tectonic evolution of the Himalayan orogen as constrained by along-strike variation of structural geometry, exhumation history, and foreland sedimentation; *Earth-Sci. Rev.* **76(1-2)** 1-131.

Zhang L K, Li G M, Cao H W, Zhang Z, Dong S L, Liang W, Fu J G, Huang Y, Xia X B, Dai Z W, Pei Q M, Zhang S T 2020 Activity of the south Tibetan detachment system: Constraints from leucogranite ages in the eastern Himalayas; *Geol. J.* **55(7)** 5540-5573.

Figure captions

Figure 1. (a) Study area shown (by the green star) on a geological map of the Himalayas (redrawn after Guillot *et al.*, 2008). **(b)** Geological map showing the Higher Himalayan litho-tectonic units exposed along the Bhagirathi River transect, Garhwal Himalaya. This map is modified and coloured after Jain *et al.* (2002). The modifications made are – Jhala Normal Fault, Harsil Formation added, and age data obtained by previous workers added on the map. The area inside the green broken box, i.e., the focus of the current study, is shown in Figure 2a.

Figure 2. Rock types in the JNF footwall. **(a)** Google Earth imagery showing the field stops and the location of the JNF. **(b)** Kyanite-staurolite-garnet schist. The garnet-bearing quartzo-feldspathic melt segregation shows a sigmoidal structure at the centre. This indicates a top-to-south shear, suggesting thrust movement. Similar smaller scale features are seen in the matrix (see the yellow box). **(c)** Tourmaline-bearing leucogranite intruded in the schist. **(d)** The melt layers in this rock are parallel to the penetrative foliation (see the lower part of the photograph). This is, therefore, a stromatic migmatite. In the upper part of the photograph, deformation becomes stronger, and the melt layers are stretched, showing the schlieren structure. **(e)** Folded layers of the migmatitic gneiss. **(f)** Augen gneiss. **(g)** Elevation profile of the river channel between locations 1 and 5. Note that the break-in elevation profile (knick point) is also marked in Figure 2a. The intersection point between the river channel and the JNF is also shown.

Figure 3. Glimpses of major features of the JNF hanging-wall (locations L4 to L5). **(a)** Remnants of the S1 foliation are present inside the prevailing S2 foliation. Note the felsic-mafic segregation banding. **(b)** Ptygmatic fold with limbs parallel to the S2 foliation. **(c)** Folds generated by S1 foliation. Note that the axial planes are sub-parallel to the S2 trends. **(d)**

Deformed quartz veins signify a vis-à-vis existence of layer perpendicular compression and layer parallel extension.

Figure 4. Examples of thrust-related (top-to-south-up) shear markers are present in the JNF hanging-wall (locations L4 to L5). **(a)** Boudinaged quartz-vein along with the foliation planes indicate a thrusting-related shear sense, **(b)** folded and sigmoid-shaped quartz vein, **(c)** tightly-folded isoclinal quartz vein, **(d)** shear boudin generated by thrusting-related antithetic shearing.

Figure 5. Sporadic occurrences of the extensional (top-to-north-down) shear markers in the JNF hanging-wall (locations L4 to L5). **(a)** thickening of the hinge and shorter limb indicating a layer perpendicular compression to be associated with the extension, **(b)** sigmoid quartz vein with sheared tails, **(c)** sheared quartz veins, **(d)** folded quartz veins are showing north-ward vergence.

Figure 6. Tourmaline-bearing leucogranite emplacement in the JNF hanging-wall (locations L4 to L5). **(a)** Lecogranite intrusion is making a low angle with the host rock schistosity. The red arrow indicates the accumulation of tourmaline at the top boundary of the intrusive. **(b)** Part of the host is completely engulfed in the intrusive body. Note the leucogranites infiltrated the fractures in the host rock and also the presence of tourmaline (red arrow). **(c)** Intrusion-induced fracture enhancement in the host. **(d)** Branch of leucogranites infiltrating a fracture at a high angle with the foliation in the host rock.

Figure 7. Mineral assemblages in the major litho units are present in the JNF footwall (a, b) and hanging-wall (c, d). **(a)** Note the presence of garnet with inclusions and **(b)** chess-board extinction in quartz (red arrow). **(c)** Micas defines the S1 and S2 foliations. The feldspar grains are more euhedral (compared to footwall), and the feldspar-feldspar grain boundaries are

meeting micas at a high angle. **(d)** presence of garnet-kyanite bearing lithounit in the hanging-wall. Bt: biotite, Grt: garnet, Ilm: ilmenite, Ky: kyanite, Ms: muscovite, Pl: plagioclase, Qtz: quartz, Ru: rutile, Tur: tourmaline.

Figure 8. Back-scattered electron images of representative monazites **(a, b)** and U−Pb concordia diagram **(c)** for samples 1105-4A collected from the JNF footwall. Back-scattered electron images of representative monazites **(d, e)** and U−Pb concordia diagram **(f)** for samples 1106-1D collected from the JNF hanging-wall.

Figure 9. Cathodoluminescence images of representative zircons from samples 1105-7 **(a-b)** and 1105-8C **(c-e),** which are from the footwall and hanging-wall of the JNF, respectively. **(f-h)** U–Pb concordia diagrams for **(f)** zircons from sample 1105-7, **(g)** zircon core and **(h)** zircon rim from sample 1105-8C.

Figure 10. Schematic cross-sections (not-to-scale) showing the geodynamic evolution of the JNF during Eocene-Miocene. LHS = Lesser Himalayan Sequence, MCTZ = Main Central Thrust Zone, HHCS = Higher Himalayan Crystalline Sequence, JNF = Jhala Normal Fault, STDS = South Tibetan Detachment System, TSS = Tethyan Sedimentary Sequence, MF = Martoli Fault. **(a)** Origin of a discontinuity at the JNF during the Oligocene HHCS channel flow. The age of peak metamorphism in the JNF hanging-wall (33.8 ± 0.8 Ma) is slightly older than that in the footwall (30.7 ± 0.5 Ma). **(a1)** Velocity profile of the channel ('pre-JNF' phase) and inception of the JNF ('syn-JNF' phase). The part (shaded grey) near the top margin of the channel is slower than the warmer central part of the channel. **(b)** Miocene rapid exhumation of HHCS triggers normal movement at the STDS. Tourmaline-bearing leucogranite intrudes the JNF hanging-wall during ~21.4 Ma. Note the melt enrichment in the JNF footwall. **(b1)**

JNF lying above the more active Miocene HHCS channel experience passive uplift during the 'post-JNF' phase.

Supplementary Tables

Supplementary Table 1. Examples of methodologies employed to obtain the age of the STDS from different parts of the Himalayas

Supplementary Table 2. SHRIMP U-Pb data of monazite

Supplementary Table 3. SHRIMP U-Pb data of zircon

Highlights

- The normal/ reverse sense of movement at Jhala Normal Fault (JNF) is controversial
- Melt proportion and shear intensity sharply decrease in JNF hanging-wall
- No extensional shear zone or break in metamorphic grade observed at JNF
- Pulsed channel in footwall causes apparent normal movement along JNF
- Normal movements along JNF and STDS are coeval with ~21 Ma leucogranite intrusion

Figure 1 new Click here to access/download;Figure;Fig. 1 new.jpg

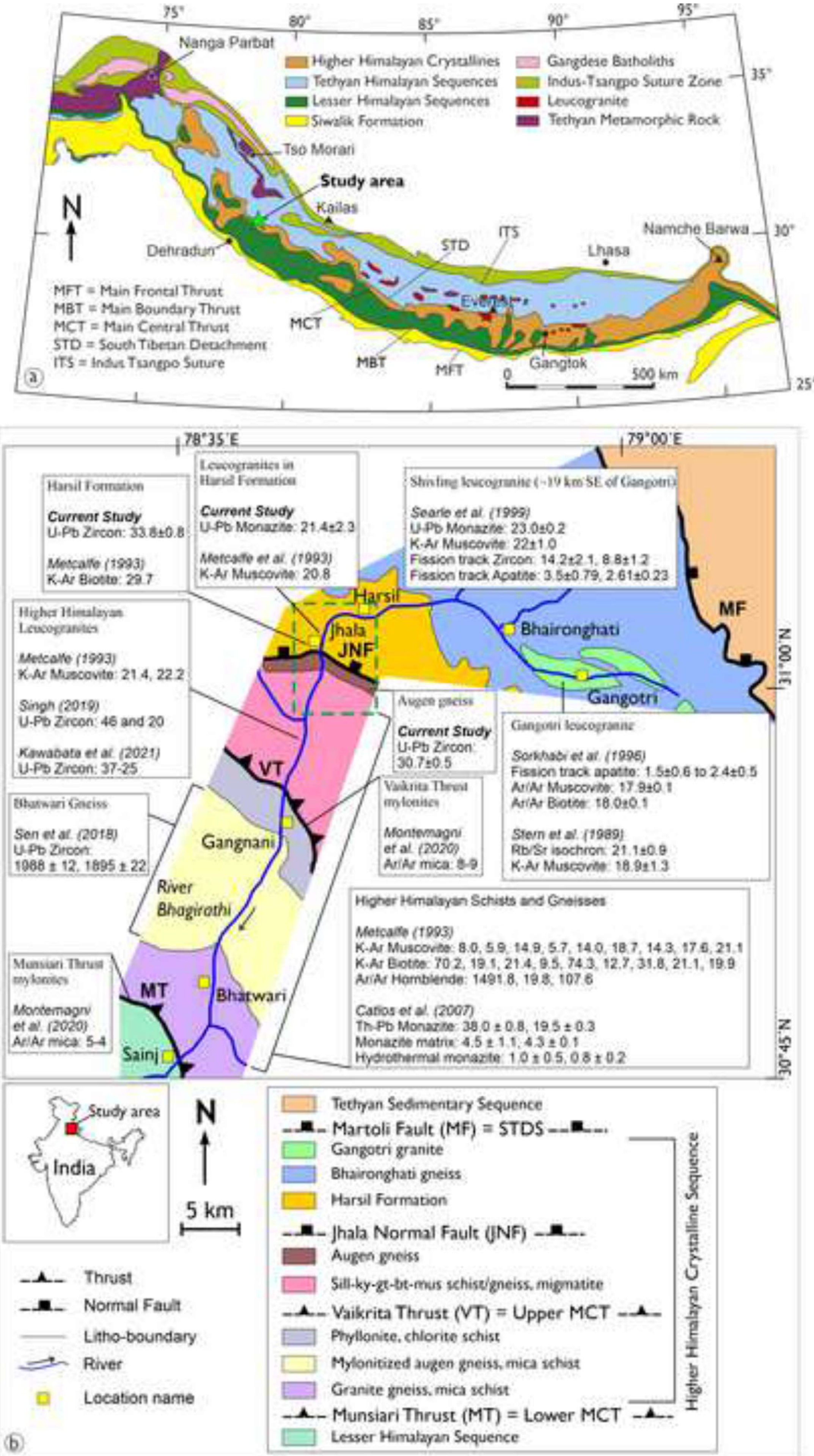

Figure 2 new

Click here to access/download;Figure;Fig. 2 new.jpg

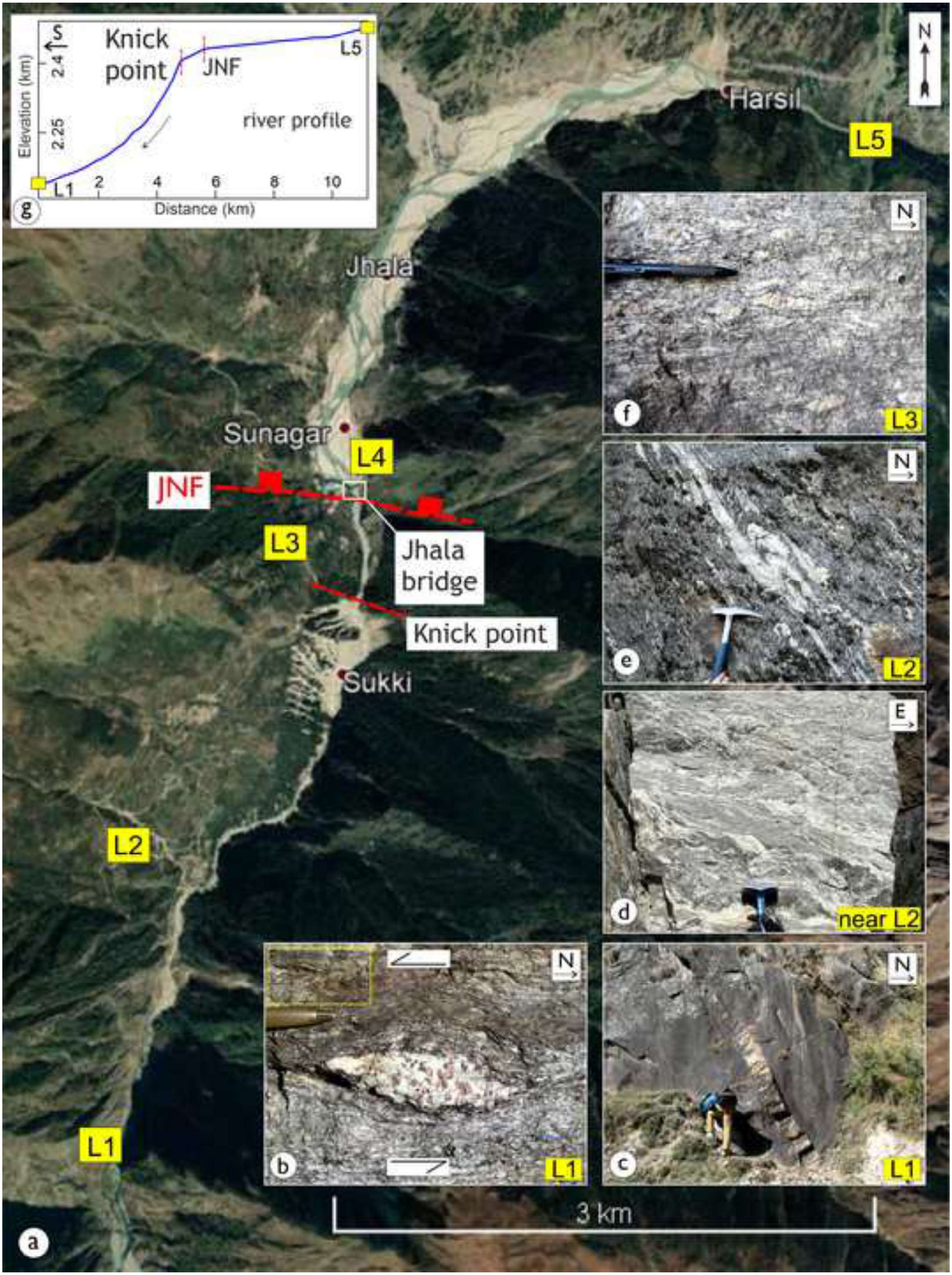

Figure 3 new

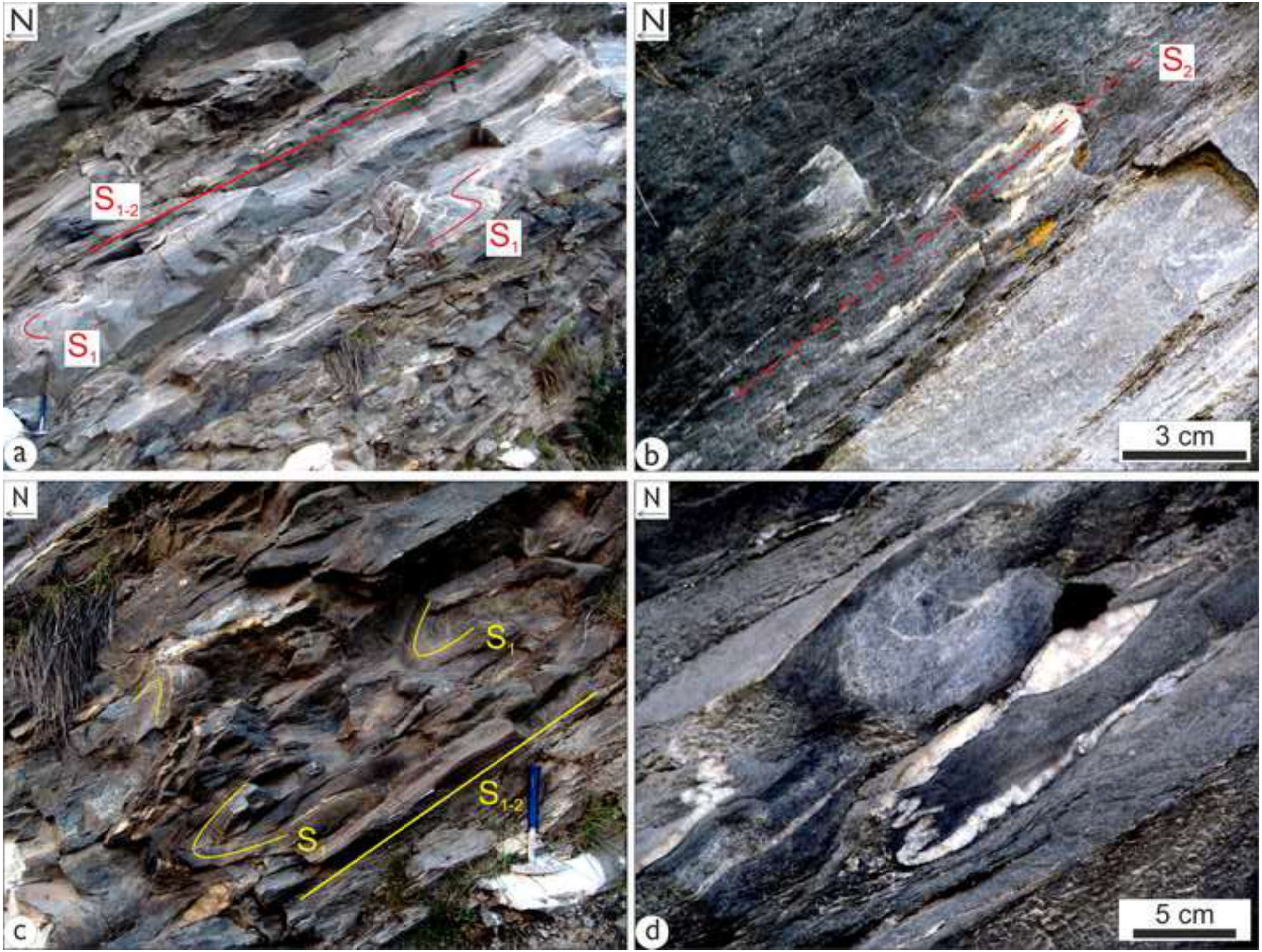

Figure 4 new

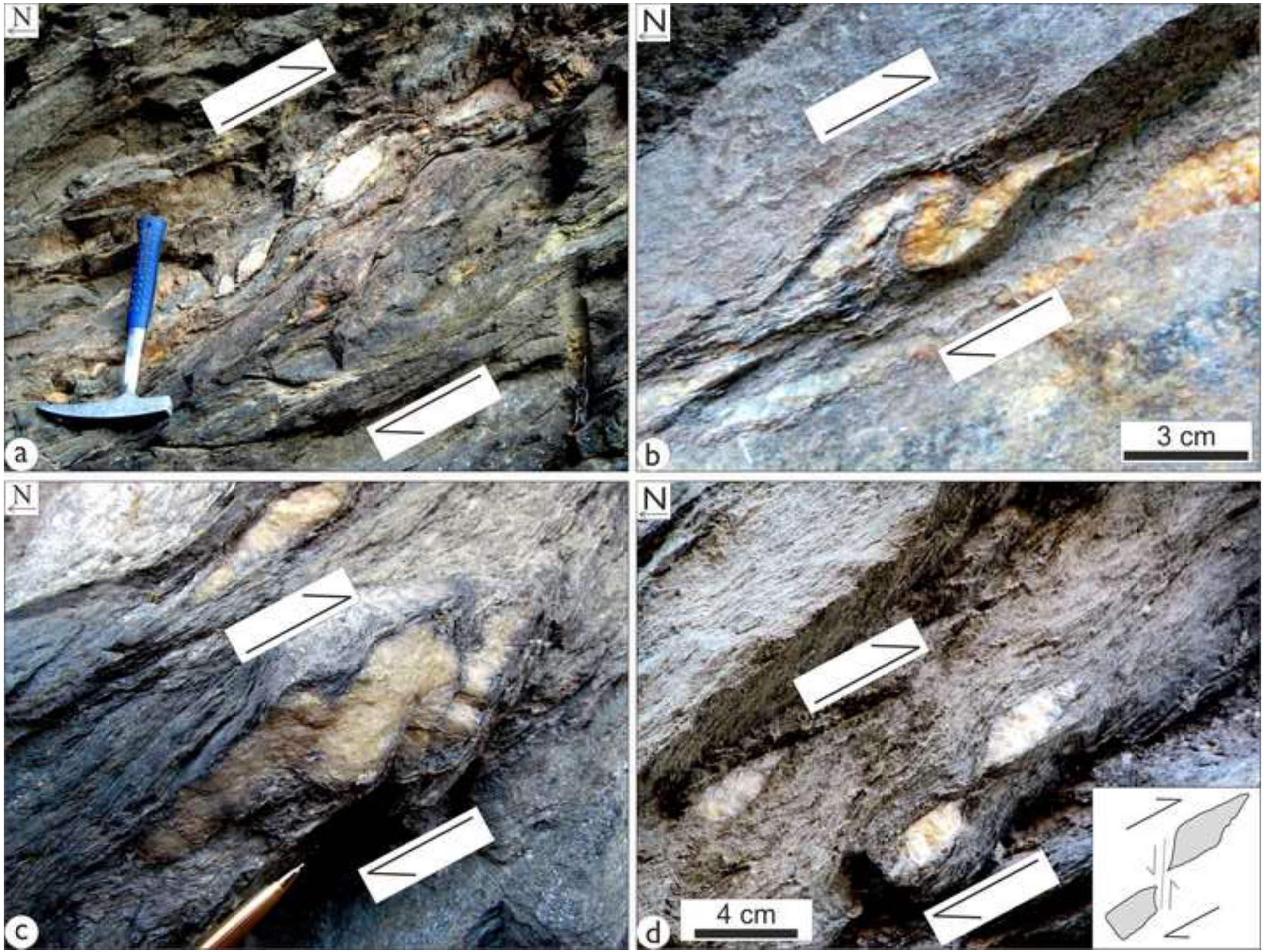

Figure 5 new

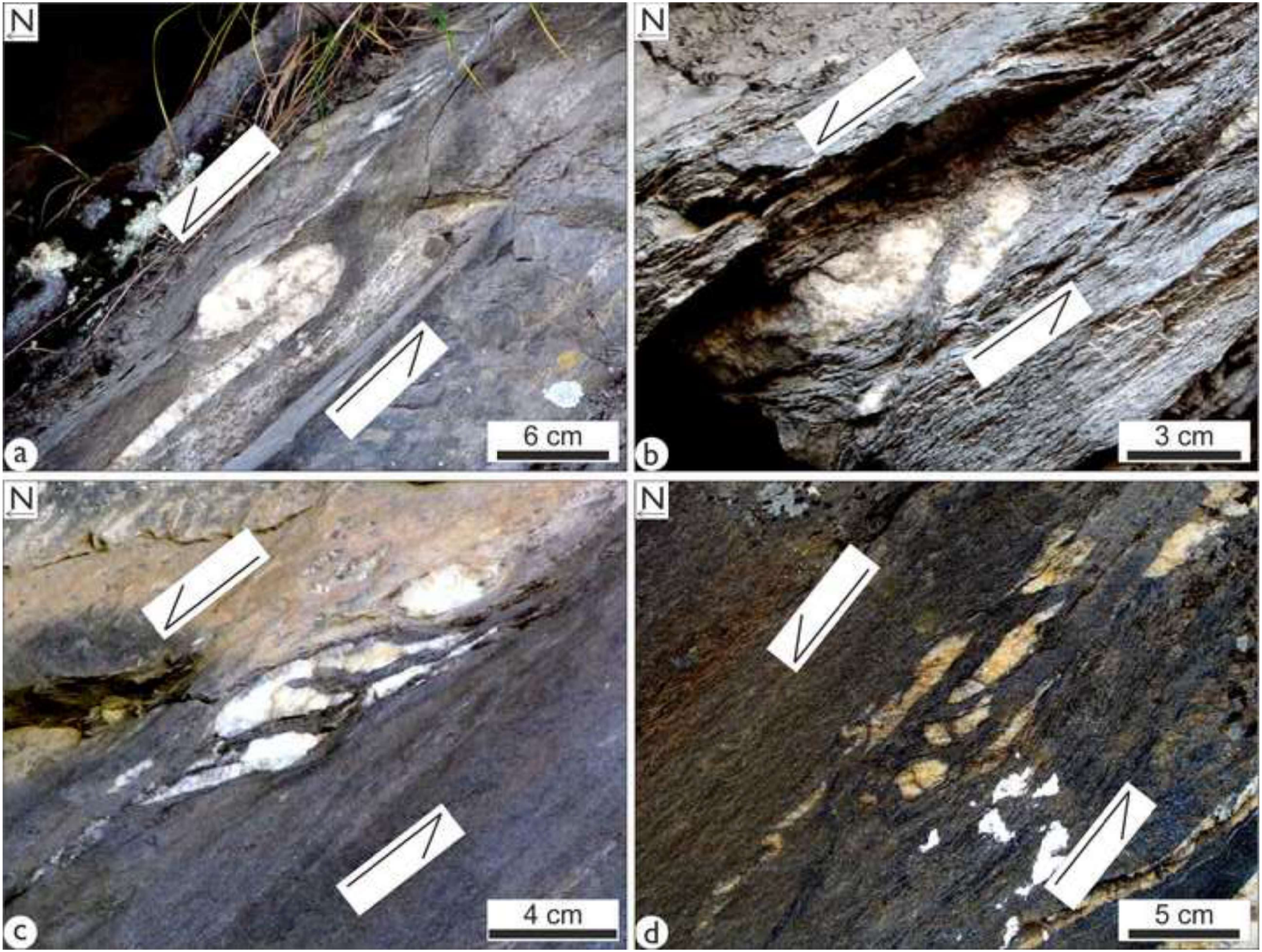

Figure 6 new

Figure 7 new

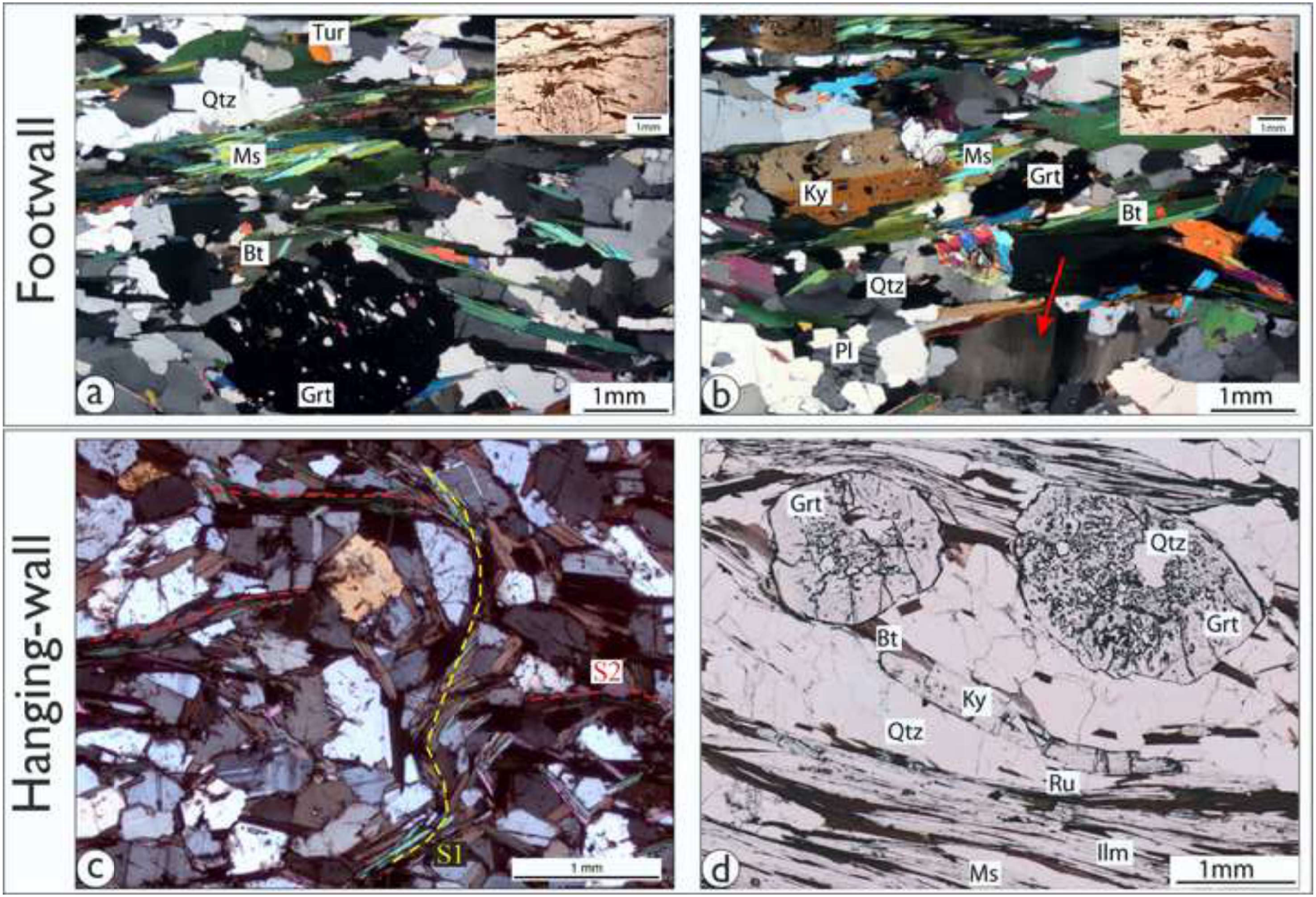
Footwall
Hanging-wall
a
Tur
Qtz
Ms
Bt
Grt
1mm
b
Ms
Grt
Ky
Bt
Qtz
Pl
1mm
c
S2
S1
1 mm
d
Grt
Qtz
Grt
Bt
Ky
Qtz
Ru
Ilm
Ms
1mm

Figure 8 new

Click here to access/download;Figure;Fig. 8 new.jpg

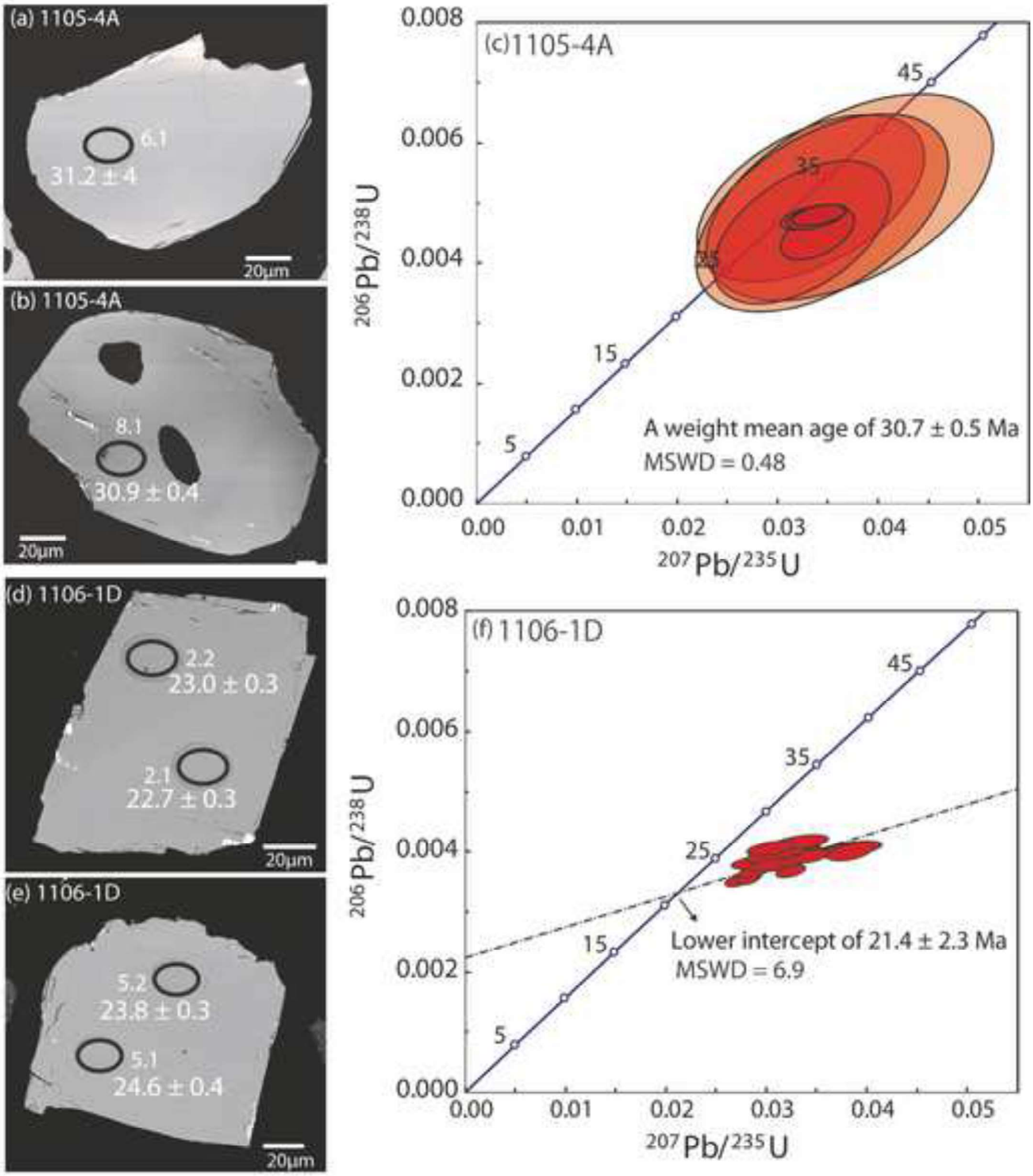

Figure 9 new

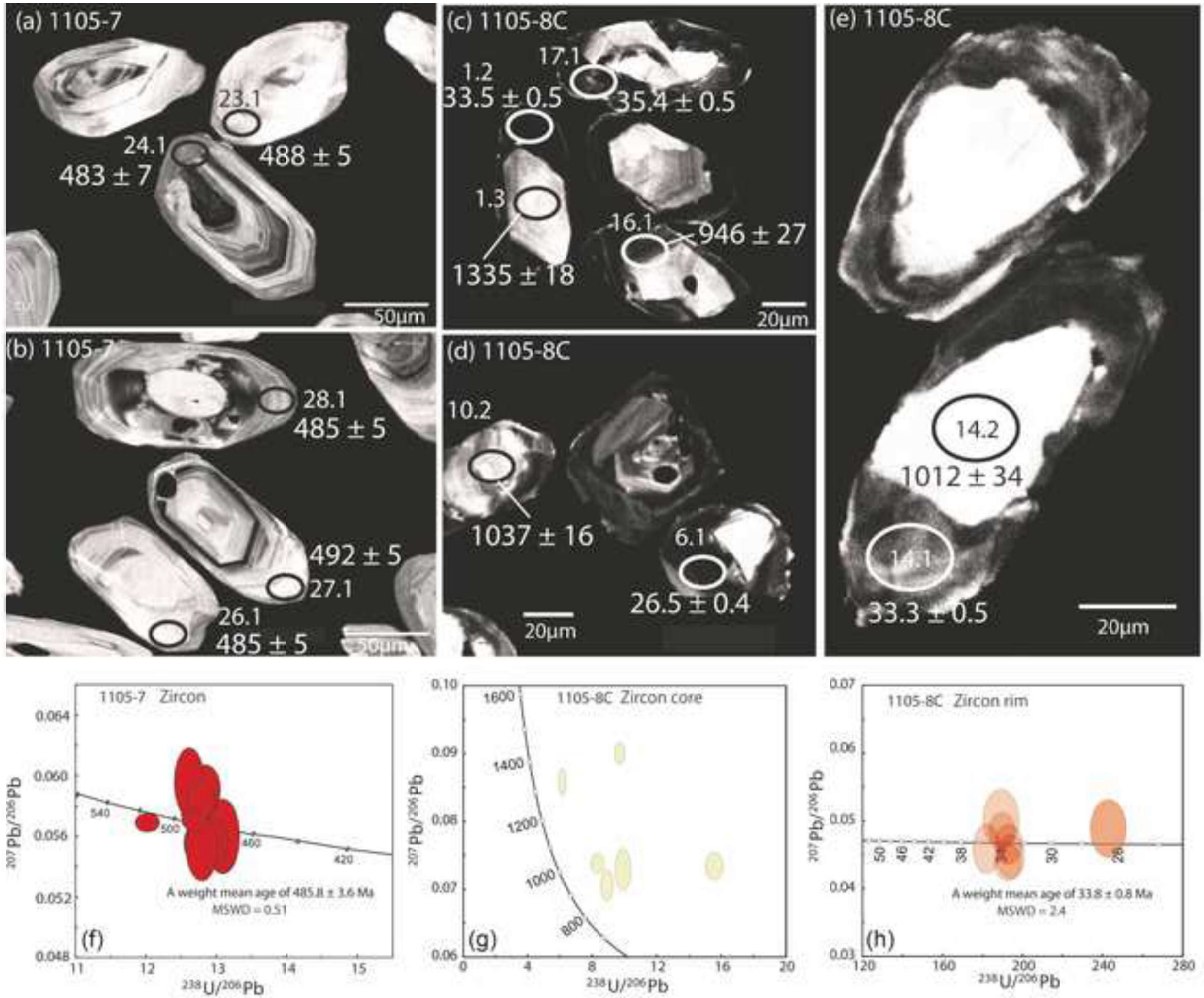

(a) 1105-7
23.1
488 ± 5
24.1
483 ± 7
50μm
(b) 1105-7
28.1
485 ± 5
492 ± 5
27.1
26.1
485 ± 5
(c) 1105-8C
17.1
1.2
33.5 ± 0.5
35.4 ± 0.5
1.3
1335 ± 18
16.1
946 ± 27
20μm
(d) 1105-8C
10.2
1037 ± 16
6.1
26.5 ± 0.4
20μm
(e) 1105-8C
14.2
1012 ± 34
14.1
33.3 ± 0.5
20μm
1105-7 Zircon
A weight mean age of 485.8 ± 3.6 Ma
MSWD = 0.51
(f)
1105-8C Zircon core
(g)
1105-8C Zircon rim
A weight mean age of 33.8 ± 0.8 Ma
MSWD = 2.4
(h)
$^{207}Pb/^{206}Pb$
$^{238}U/^{206}Pb$

Figure 10 new Click here to access/download;Figure;Fig. 10 new.jpg

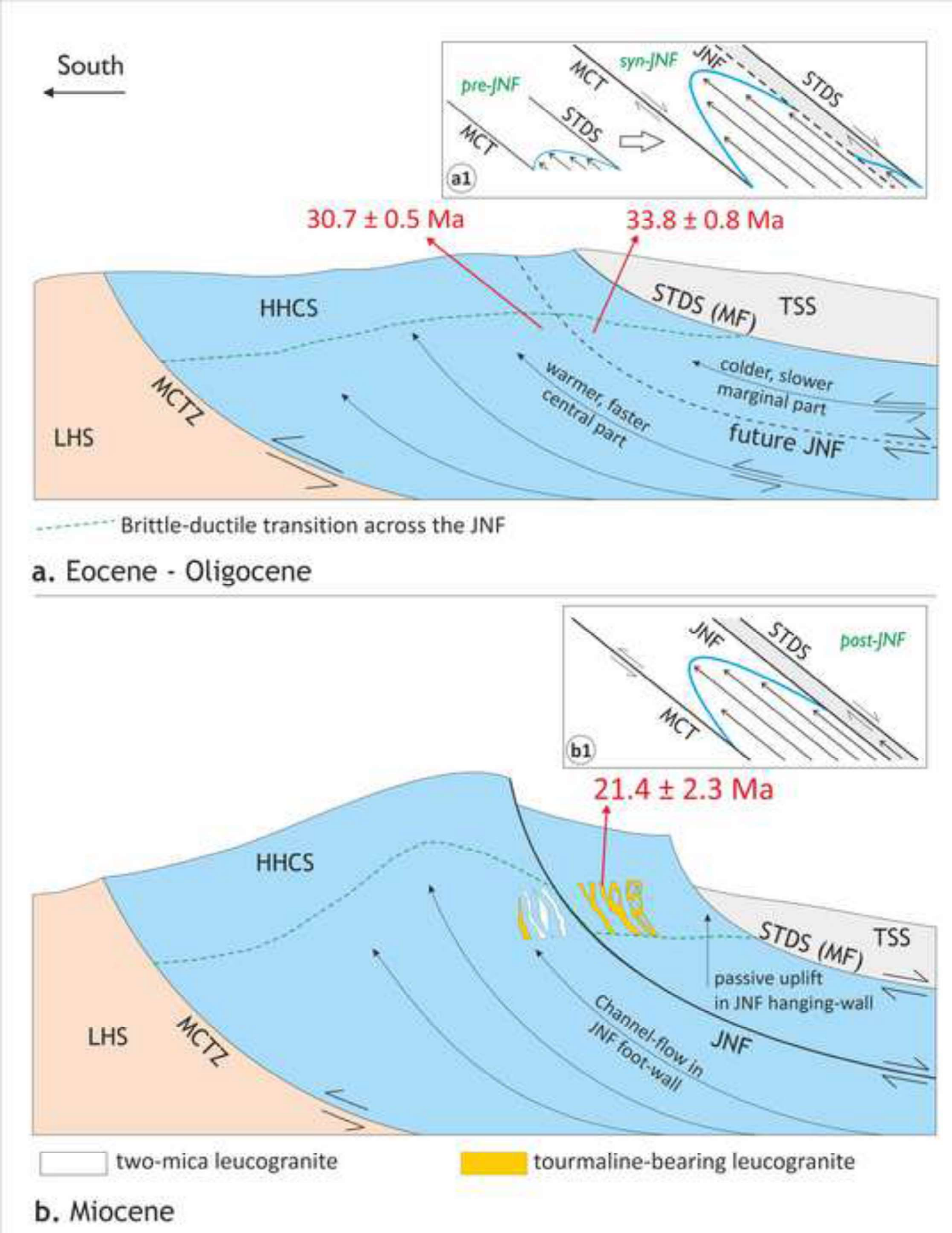

Supplementary Table 1

Supplementary Table 2

Click here to access/download
Electronic Supplementary Material
Supplementary Table 2_Monazite U-Pb ages.docx